Development, Optimization and Test Performance of Highly Efficient Flat Plate Solar Collector with Transparent Insulation and Low-Cost Overheating Protection

Deniz Kizildag[1], Jesús Castro[1], Hamdi Kessentini[2], Joaquim Rigola[1] and Assensi Oliva[1]

[1]Heat and Mass Transfer Technological Center (CTTC)

Universitat Politècnica de Catalunya-BarcelonaTech (UPC)

ETSEIAT Colom 11 08222 Terrassa, Barcelona, Spain

cttc@cttc.upc.edu, http://www.cttc.upc.edu

[2]Université de Tunis El Manar, Ecole Nationale d'Ingénieurs de Tunis (ENIT)

Laboratoire de Matériaux, Optimisation et Énergie pour la Durabilité (MOED), 1002 Tunis, Tunisia

Abstract

The present work addresses a flat plate solar collector with transparent insulation material (TIM) and high temperature protection system. The design and optimization of the collector have been numerically carried out by means of a parallel object-oriented simulation tool which is capable of simulating all the entities constituting the system as a whole, using efficient coupling between the elements. Three variants of the design are chosen to first test them under laboratory conditions. These collectors then are mounted in the roof of a hospital building, where their performance are comparatively tested along with a conventional flat plate solar collector, under real meteorological conditions and during long periods of time. Thus, due to long term exposure of the collectors, aspects such as reliability, durability, energy performance, correct functioning of the protection system will be analyzed, with the objective of improving the detected shortcomings for the future generations of the present design.

Keywords: Flat plate solar collector, thermal insulation material, thermal protection system, collector testing

1. Introduction

Flat plate solar collectors are generally designed for working temperatures between 40 and 60 ºC, which makes them ideal for their application in domestic hot water systems. Despite the variety of the products which have appeared in the market dedicated to the solar energy capturing, flat plate solar collectors have a privileged share in the market due to their simplicity, relatively lower cost, ease to manufacture, and the capability to collect radiation being stationary in any roof. By using highly selective absorbers, these collectors can work at temperatures up to 80 ºC with good efficiency (Kalogirou, 2003). To extend the application of these devices to higher working temperature, thus making them more available for applications such as food, drying of wood, crops, fruits, distillation, desalination, solar cooling (Nkwetta and Smith, 2012; Sharma et al., 2017), the transparent insulation materials (TIM) between two transparent covers or between absorber and outer glazing were used (Rommel and Wagner, 1992; Platzer, 1992). In some of these works, glass capillary tubes were considered, which despite their good resistance to temperature, increased the cost and weight of the collectors considerably. For commercial solar collectors, plastic TIM is potentially a good solution due to its advantage over glass capillary tube solution in terms of cost and weight. The main drawback is its vulnerability under the stagnation conditions. To overcome this problem, different solutions were proposed. Martínez et al. (2013) proposed a thermoelectric self-cooling system designed to dissipate the excess heat. A flat plate collector with plastic TIM and passive overheating system based on closed loop heat-pipe was recently introduced to the market showing good thermal performances (Adel, 2013).

In the present work, a flat plate solar collector with transparent insulation material is addressed. The scheme of the collector is shown in Fig. 1. The collector aims at delivering heat at the range from 80 to 110 ºC. The losses due to natural convection between the absorber plate and the cover glass is expected to be reduced due to employment of a layer of cellulose triacetate honeycomb TIM. According to the TIM manufacturer, this material can typically withstand a temperature of 140ºC, which can easily be reached under stagnation conditions. Indeed, yellowing and embrittlement can already be observed at temperatures above 100°C, well below the expected temperatures according to manufacturer's data. Moreover, outgassing, which affects both the optical efficiency and the appearance of the

doi:10.18086/swc.2017.31.07 Available at http://proceedings.ises.org

collector, may occur at temperatures below 100 °C (Giovannetti et al., 2011). Thus, to protect TIM, the collector involves a ventilation channel between the absorber and back insulation, which operates thanks to a thermally actuating door which uses a shape memory alloy. When the system reaches high temperatures, the door opens, thus ventilating the collector to safer temperature levels. The collector is designed by means of a numerical model based on the numerical resolution of different components of the collector in the framework of a modular, object-oriented platform. The design is first tested in laboratory conditions, where the correct functioning of the system is tested and the characteristic curve of the collector is obtained. During the laboratory tests, different issues related with TIM and overheating protection system are identified and improved. The tested prototypes are then installed in the roof of a hospital building, where they are used along with the conventional flat plate solar collectors to cover the domestic hot water and space heating demand of the building. The site is properly instrumentalized so as to compare both developed and commercial collectors in terms of energy performance. Moreover, the prolonged exposure of the prototype under real climatic and working conditions constitutes a useful test for the reliability and durability of the design.

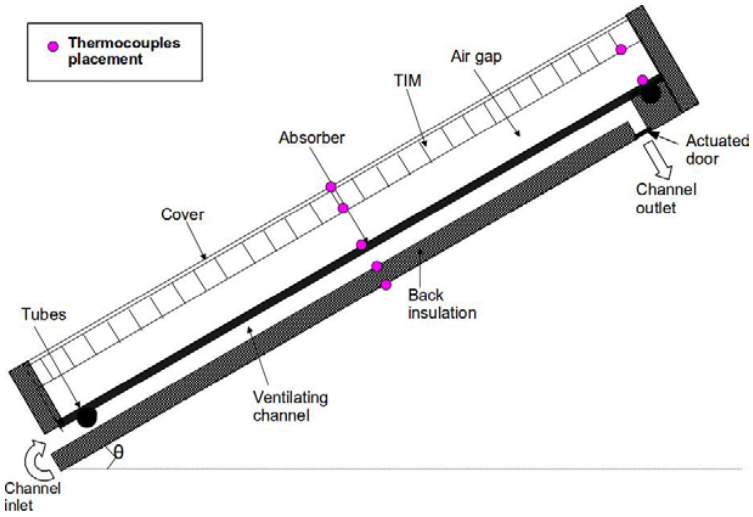

Fig. 1 Schematic view of the flat plate solar collector with TIM and ventilation channel.

2. Mathematical and numerical method

A mathematical model was developed (Kessentini et al., 2014b) where the flat plate solar collector with TIM and thermal protection can be numerically studied. In this model, the thermal and fluid dynamic phenomena taking place in each of the components that make up the prototype, i.e., glass cover, TIM, air gap, absorber plate, working fluid, ventilation channel, opaque insulation material, are numerically resolved considering different levels of complexity. In Figure 2, the detail of the mathematical model and the heat flux terms considered in the cross-section of the prototype and the absorber are schematically depicted.

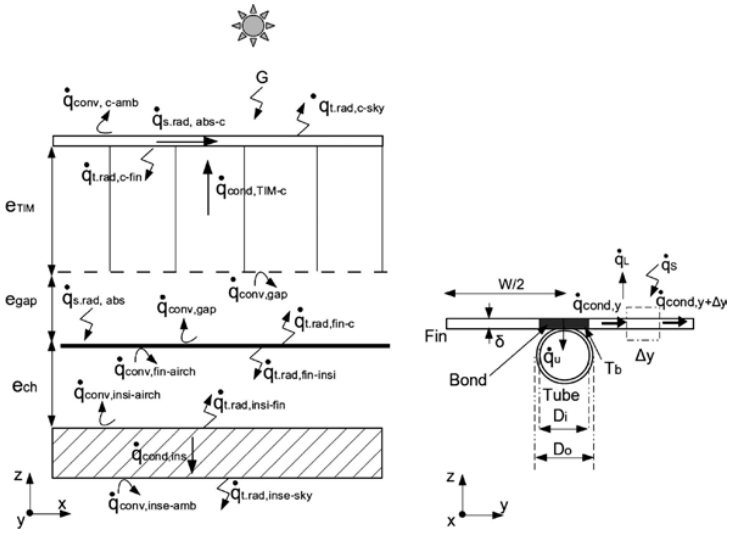

Fig 2. Detail of the heat flux terms. A cross section of the collector with TIM (left) and heat transfer at the absorber (right).

The object-oriented platform, called NEST (López et al., 2012), enables proper interaction between related components. The components, which can be treated as independent objects, can be linked with other related components through a global resolution algorithm. The numerical platform allows for efficient communications between the components (see Figure 3). Depending on the desired level of detail in the resolution of a particular element, even a high-level CFD object can be employed in the resolution of parts of the system. Given the computationally demanding nature of such a system composed of one or more CFD objects, the NEST framework provides parallelization to distribute the available computational power depending on the demands of each component, thus reducing computational time. Besides the active solar energy systems, like flat plate solar collectors (Kessentini et al., 2014a), this framework was also employed in the study of passive systems (Kizildag et al., 2014). Further details of the mathematical and numerical model used in this study are presented in Kessentini et al., 2014b.

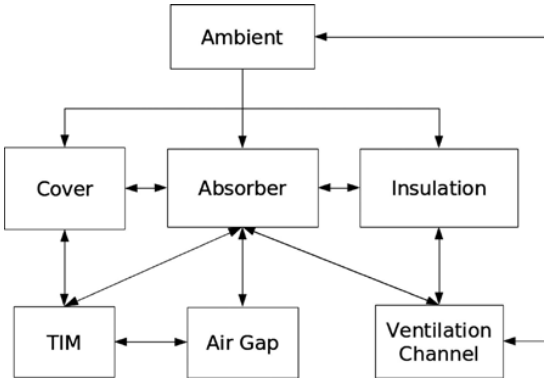

Fig. 3 Representation of the system composed of different components and their communications between each other.

3. Lab-scale testing and improvements

In line with the outcomes of the predesign performed using the numerical tool, prototypes with different TIM layer thicknesses were initially considered to observe their influence on the overall performance. In order to perform the characterization of the optical properties of the selected options, a set of preliminary glass-TIM configurations were initially tested under real outdoor conditions, as shown in Figure 4.

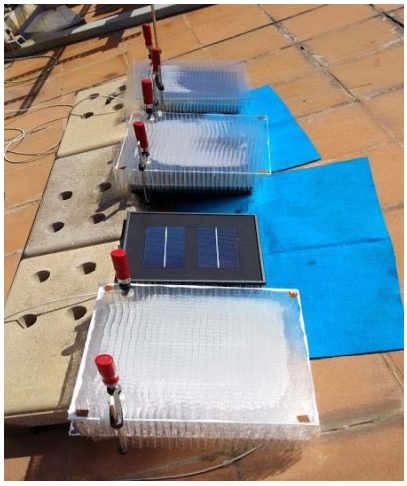

Fig. 4 Transmittance test set-up for different glass-TIM configurations under real climate conditions

As a result of previous analysis, and considering the numerical results, prototypes with four different TIM layer thicknesses (40mm, 50mm, 60mm, and 75mm) were manufactured to observe their influence on the overall performance. These prototypes were tested in the CTTC Solar Cell (see Figures 5 and 6), where tests up to 150 ºC and 8 bars can be performed using pressurized water. This experimental infrastructure allows for a comparative test employing two collectors in a parallel configuration.

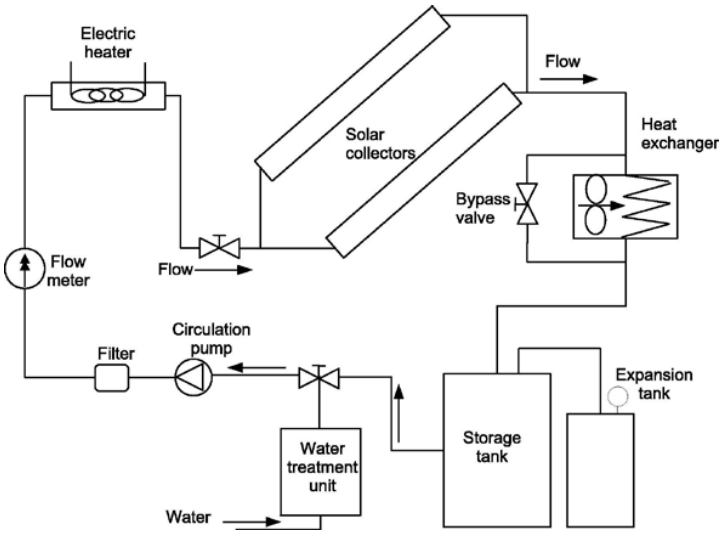

Fig. 5 Schematic view of the CTTC Solar Cell.

The main elements of the CTTC Solar Cell are the heater, water pump, filter, visor, expansion vessel, regulation and mixing valves, Coriolis flowmeter, storage tank, water treatment unit, heat exchanger, pyranometers for total and diffuse radiation in the plane of the tested collector, cup anemometer, 2D ultrasonic anemometer, temperature sensors, air vents. Some of these elements can be visualized in Figure 6. The experimental data is gathered using a data acquisition system, composed of a PC, an HP 3852A and two Agilent 34970A data acquisition units.

Fig. 6 Pictures of the key elements constituting the CTTC Solar Cell.

The manufactured prototypes are first subjected to the stagnation test, which is carried out to determine the maximum

temperature the collector can reach in the absence of mass flow. As no heat is transferred to fluid, the internal energy of the solar collector gradually increases, finally rising the temperature of the system up to an elevated temperature. It has been observed that the collector reached at the temperature of approximately 108 ºC when the thermally actuated door opened and started to cool down the collector. At that moment, TIM temperature was observed to be approximately 95ºC, which is well below the maximum temperature this element can resist. Visually inspecting the collector, TIM apparently was not damaged during the stagnation test, confirming that the effectiveness of the overheating protection system. In Figure 7, different temperatures registered during the stagnation test of a first generation prototype is depicted.

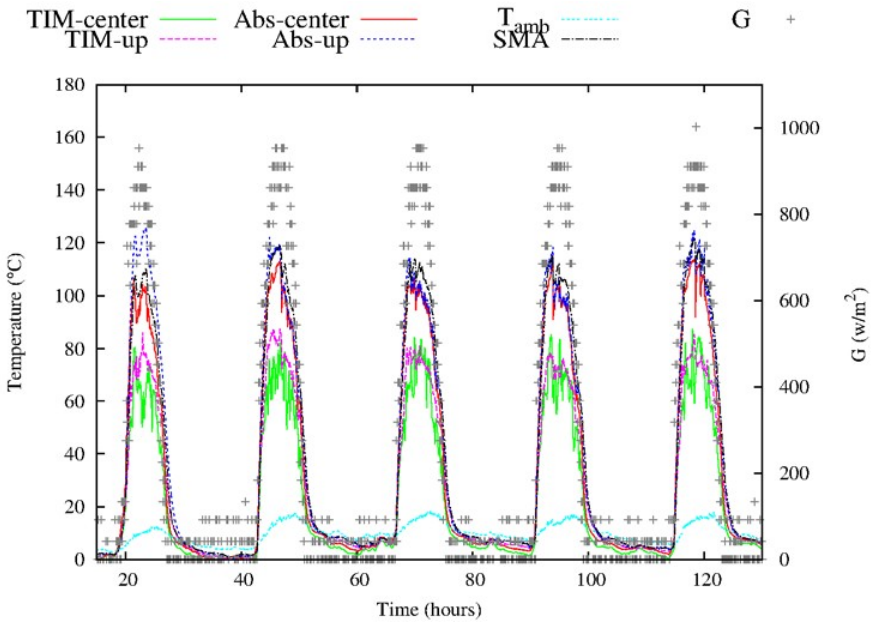

Fig. 7 Temperatures corresponding to different locations of TIM, absorber plate, sma spring, outdoor and total radiation on the tilted plane of collector registered during the stagnation test for an initial prototype.

After confirming that the prototypes are stagnation-proof, the outdoor steady-state efficiency test was performed following the recommendations of the international standard procedure described in ISO 9806-1. Accordingly, the prototypes were exposed to outdoor conditions for prolonged periods of time, assuring a constant temperature of the collector at the inlet. A mass flow rate of 0.042 kg/s was employed considering the collector absorber area. The collector is tested at 35, 50, 70, 90, and 110 ºC. The measurements obtained in periods close to solar midday are selected in order to fulfill criteria related with the angle of incidence. Other criteria regarding the amount of total solar radiation, the percentage of diffuse radiation, permitted variations in outdoor temperature and collector inlet temperatures throughout the test period are carefully attended. As the test were carried out under real climatic conditions in outdoors, it was not always possible to obtain favorable conditions for the collector testing. This caused requiring an important period of time to conduct the experiments and having to repeat the tests at different inlet temperatures.

The manufactured prototypes are tested in lab-scale where some of the shortcoming of the design were detected and improved, such as the condensation phenomenon observed due to the humidity absorbed by the plastic TIM material (see Figure 8). This problem was solved by means of introducing small ventilation holes, thus improving the ventilation and reducing the differences between the micro-climate of the collector and the outdoor ambient conditions. During the lab-scale tests, the emphasis is given to the influence of TIM material

Functioning of the thermally actuating door system is adjusted, with the objective of improving the phenomenon of premature opening of the channel. An experimental trial-error procedure was followed in order to determine the location and configuration of different elements constituting the overheating protection system, to make sure that thermally actuated spring is able to activate the ventilation channel under stagnation conditions while the channel can effectively be deactivated as the system is cooled down as a result of the heat evacuation by means of the ventilation channel.

Attachment of the TIM layer to the glass has been secured by more effective mechanisms, avoiding detachment of the cheap transparent insulation material under extreme conditions.

Fig. 8 Condensation phenomenon observed in a preliminary prototype

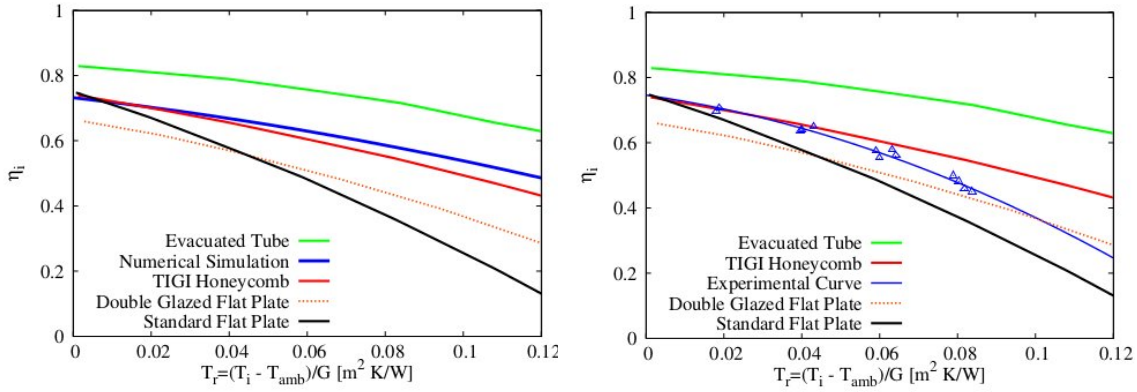

Fig. 9 Numerical (left) and experimental (right) steady-state efficiency curves of the prototype with 60mm TIM compared with solutions in the market.

In Figure 9, both numerical and experimental results during lab-scale tests are presented. The experimental curve corresponding to a first generation of prototypes is depicted in this graph. Note that these results anticipate an improvement with respect to the standard flat plate solar collector, at only slightly higher cost, since both TIM and overheating protection system use low-cost materials. The prototype achieves a somewhat lower performance with respect to the evacuated tube collector, though this type is expected to be approximately twice as costly as the manufactured prototype. In order to achieve the theoretical expected performance, improvements were implemented, especially affecting the insulation of the whole collector.

After the improvements with respect to the first generation of prototypes, a second generation was manufactured. In this second generation, a TIM layer of 75mm was used. This collector was also tested in laboratory conditions, obtaining finally the following steady-state efficiency curve given in eq.1:

$$\eta_i = 0.698 - 0.985\frac{(T_i - T_{amb})}{G} - 0.025\frac{(T_i - T_{amb})^2}{G} \qquad \text{(eq. 1)}$$

This curve is depicted comparatively in Figure 10, together with the curves of the previous generation of prototypes and commercial flat plate solar collector with TIM (TIGI LTD., 2011).

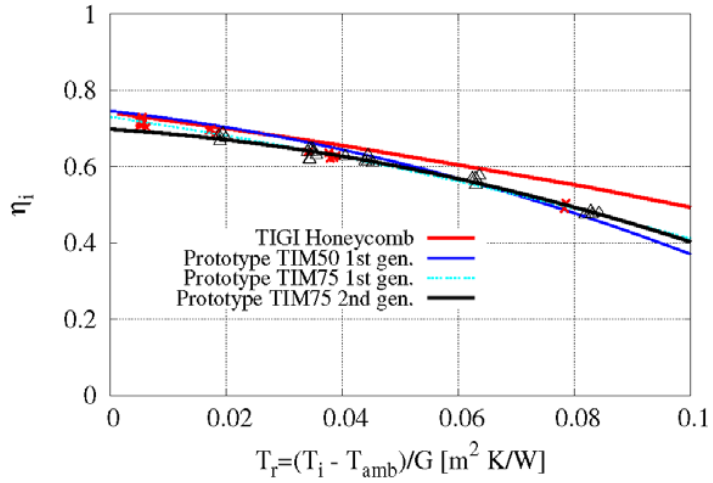

Fig. 10 Steady-state efficiency curves of different prototypes, compared with commercial flat plate solar collector with TIM.

Considering that the prototype involves a layer of TIM, it is of interest to the analyze the influence of the angle of incidence on the performance. Note that the steady-state efficiency curve is obtained for irradiation at or near normal incidence conditions. To that end, the prototype with TIM75mm is tested in outdoor conditions for a set of days in summer and autumn, always in clear sky conditions. In Figure 11, the results of the incidence angle modifier test are depicted. The experimental results reveal that the optical effects penalize the collector of the order of approximately 7 %, 10 %, and 32 % for the angles of incidence of 30º, 45º, and 60º, respectively. The methodology followed was to obtain the efficiencies for steady-state periods of 15 minutes, for symmetric intervals of time before and after solar midday, assuming an average angle of incidence of the given interval, and comparing it with the normal incidence efficiency for that particular conditions.

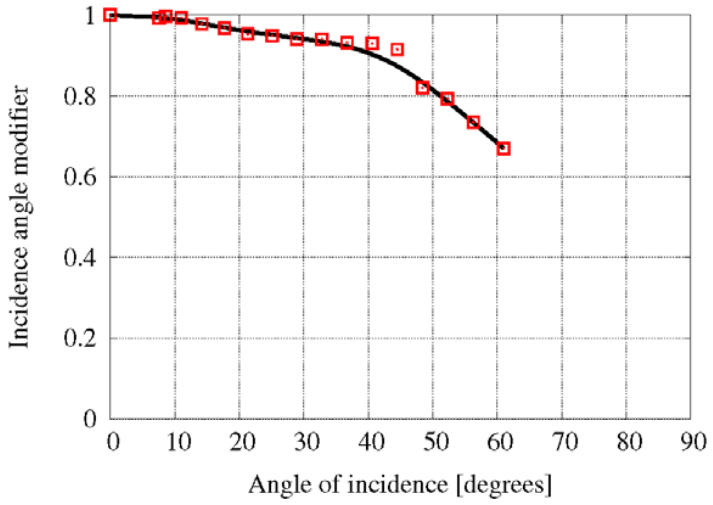

Fig. 11 Incidence angle modifier of the Prototype with TIM75mm, obtained by outdoor testing using a stationary test rack.

4. Long-term performance in demo site

Three prototypes, only differing in the TIM layer thickness (40mm, 50mm, and 60mm) are installed in the roof of a hospital building close to Barcelona (see Figure 12), where they are being tested comparatively with a commercial flat plate solar collector under real working and meteorological conditions during prolonged periods of time. The commercial collectors installed in the roof of the demo building do not have a layer of TIM. The steady-state efficiency curve provided by the manufacturer is given in eq. 2:

$$\eta_i = 0.739 - 3.706\frac{(T_i - T_{amb})}{G} - 0.017\frac{(T_i - T_{amb})^2}{G} \qquad \text{(eq. 2)}$$

The site is instrumentalized by means of mass flow, temperature, and radiation sensors. The long-term performance test in demo site provides realistic data for the functioning of the solar collectors, especially considering the solar heat delivered to the system and the reliability of the prototypes during prolonged periods of time. In the present work, demo site performance of the collectors are analyzed for winter and spring conditions.

Fig. 12 Solar energy capturing field of the Albada Building in Parc Tauli Hospital. The three prototypes are tested alongside the conventional flat plate solar collectors without TIM.

4.1 Winter Performance:

The prototypes, due to the employment of TIM are expected to have improved performance with respect to the standard flat-plate solar collectors, especially under the winter conditions where the losses to the ambient are pronounced as a result of important temperature gradient between intermediate collector working temperatures and outdoor conditions. In Figure 13, the ambient temperature and the total solar radiation on the plane of the collectors are depicted for a typical sunny day in the demo site location. Considering that the temperature in the inlet of the collectors was between 65-70ºC for this period, which is optimized considering the domestic hot water and space heating system installed in the hospital services building, important losses to the ambient can be anticipated.

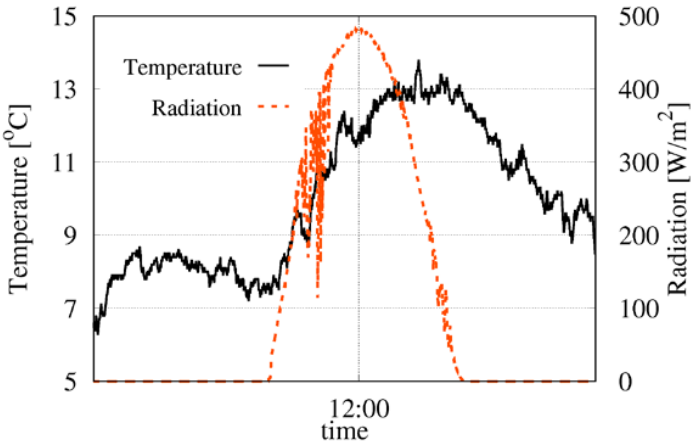

Fig. 13 Ambient temperature and solar radiation in the plane of the collectors for a sunny day in January 2017, mesured in Parc Tauli.

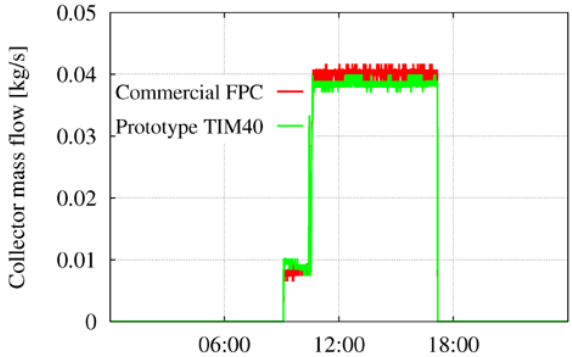

Fig. 14 Mass flow through the prototype and commercial flat plate collector without TIM for a representative sunny day in January 2017.

Note that the solar energy capturing circuit is activated only when a critical solar energy availability is reached. See Figure 14 for the registered mass flow through a prototype and a conventional flat plate solar collector without TIM.

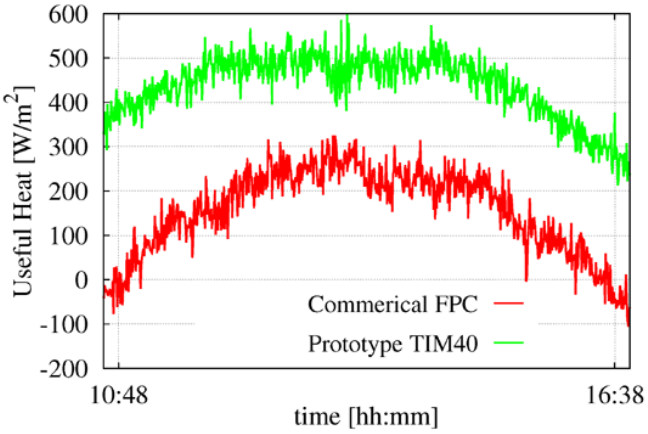

Fig. 15 Delivered useful heat for a representative day in January 2017 for the compared collectors.

In Figure 15, instantaneous useful heat delivered to the system is depicted both for the prototype and conventional flat plate collector without Tim for the day represented in Figure 14. This figure indicates a substantially better performance of the prototypes with TIM with respect to the conventional flat plate collectors, especially in winter conditions, when the losses from the collectors to the ambient are naturally enhanced, and the demand for space heating and domestic hot water is relatively higher.

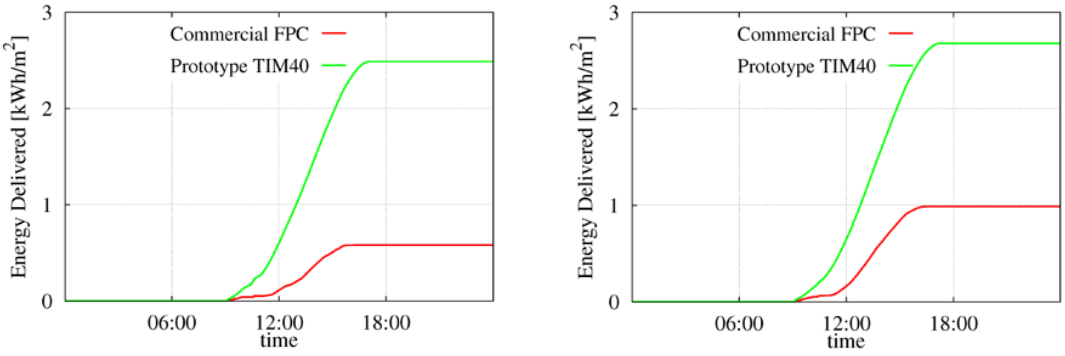

Fig. 16 Accumulative energy delivered to the system by the prototype and conventional flat plate collector without TIM for consecutive days in winter.

The trend captured in Figure 15 can be observed for other days during winter period of dissimilar solar availabilities, as shown in Figure 16, where the accumulative energy delivered to the system by the two compared collectors are depicted.

The steady-state efficiency curves of the collectors give valuable information on the thermal behavior of the collector under steady-state conditions with near-to-normal solar angle of incidence, together with some other additional conditions. However, a daily average collector efficiency can be defined, based on the energy delivered during the whole day by a collector and the solar energy available on the collector surface. Note that, this daily average efficiency will naturally have lower values with respect to the corresponding efficiencies indicated by the characteristic curve of the collector, as the curve is obtained by considering only the optimum conditions. Using the average data obtained in the vicinity of these days, which indeed are close approximation of the average day of the month considering the declination angles of the sun for this month, the daily average efficiencies for the prototype and conventional flat-plate collector are found as 41% and 16%, respectively.

In the absence of continuous readings due to technical problems in the demo site, these observed daily average efficiency values can be employed to obtain an approximation of the energy savings by both collectors for the winter meteorological conditions of the demo site. In Table 1, the total solar radiation in the vicinity of the demo site is provided, using the database of Meteonorm © software. The present estimation anticipates important savings as the high efficiency solar thermal collectors are employed for the given working conditions of the demo site.

Tab. 1: Total radiation on the inclined surface of the collectors and the estimated delivered heats during winter months.

Month	Total Radiation on Titled Plane (kWh/m^2)	Energy Delivered by Commercial Collector (kWh/m^2)	Energy Delivered by Prototype (kWh/m^2)
December	111	17.76	45.51
January	123	19.68	50.43
February	131	20.96	53.71
Winter Total	365	58.40	149.65

4.1 Spring Performance:

During the months of Spring, some experimental data could also be gathered in the demo site. Note that, due to relatively increased ambient temperatures, general losses of the collectors are reduced with respect to those in the winter season. Collectors are expected to work at higher efficiencies, which, especially in the case of the conventional collector, is expected to close the gap with the prototypes employing TIM.

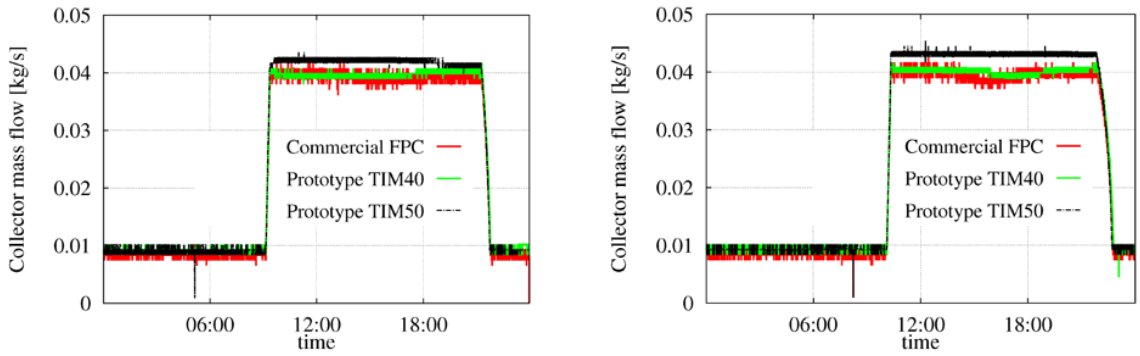

Fig. 17 Mass flow through two prototypes (TIM40 and TIM50) and commercial collector without TIM for two days with solar avaliability in March 2017.

In Figure 17, mass flows passing through the analyzed collectors are depicted for March 2017. Note that, due to requirements of the installer of the hydraulic circuit, the mass flow was not set to zero during periods of insufficient solar radiation. In the calculation and comparison of the accumulated energy delivered to the system by the analyzed collectors (see Figure 18), the effect of the nighttime flow was not taken into account, as it is considered as a temporary practice.

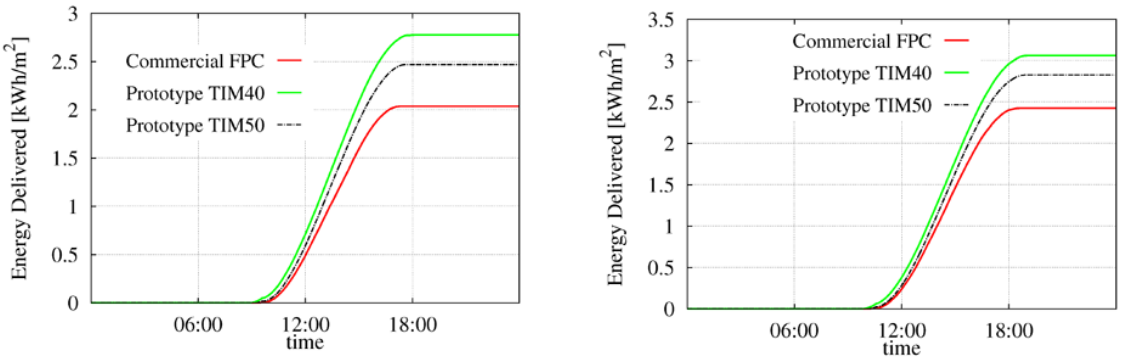

Fig. 18 Accumulative energy delivered to the system by the prototypes (TIM40 and TIM 50) and commercial flat plate collector without TIM for two representative days with solar availability in March..

Note that the commercial flat-plate collector improves its performance with respect to the winter period, even though it still delivers less amount of energy per area when compared with the prototypes. 40mm TIM layer prototype was observed to show better performance. Following the previous approach for defining an average efficiency for the

collectors based on these two test days, daily average efficiencies of 43% and 31% are obtained for 40mm layer TIM collector and commercial flat-plate collector, respectively. This information is used to estimate the delivered energies per area for both collectors during the tested spring period, as shown in Table 2.

Tab. 2: Total radiation on the inclined surface of the collectors and the estimated delivered heats during spring months.

Month	Total Radiation on Titled Plane (kWh/m^2)	Energy Delivered by Commercial Collector (kWh/m^2)	Energy Delivered by Prototype (kWh/m^2)
March	165	51.15	70.95
April	168	52.08	72.24
May	173	54.68	73.40
Spring Total	506	157.91	216.59

5. Conclusions

It has been demonstrated that different variants of the designed prototypes are capable of delivering higher amounts of heat to the domestic hot water and space heating system of a specific hospital building when compared with the conventional flat plate solar collector. The employment of the designed novel collector is especially interesting for the present application, as the practical working temperatures give rise to important losses during winter periods. The visual inspection of the prototypes does not present any issues related with ageing of TIM, problems with TIM adhesion, any damage of TIM due to stagnation conditions, which indicate a proper functioning of the overheating protection system. It is worth noting that due to the faults registered in different elements of the circuit, not necessarily related with the solar energy capturing field, the hydraulic circuit of the system did not function during prolonged periods of time in spring and summer. Thus, it can be stated that, this circumstance provided the necessary exposure of the designed prototypes to the stagnation conditions, building confidence in the reliability of the prototype collectors.

Thus, although the tested period does not yet cover a representatively long time span, the initial outcomes indicate promising results in terms of both energy efficiency and reliability of the present design.

6. Acknowledgments

This work has been financially supported by the European Community FP7 Programme, EeB.NMP.2013-3 No 609377 “RESSEEPE Project”. The authors thankfully acknowledge this support.

The authors would also like to acknowledge Manuel Ordoño, Cristóbal Galleguillos for their technical support during the lab-scale tests; and *Consorci Corporació Sanitària Parc Taulí de Sabadell* for their support and contributions in the building of the experimental facility in the demo site.

7. References

Adel M., 2013. Honeycomb collectors for high temperature differential solar thermal applications. In: International conference on solar heating and cooling for buildings and industry [ref:47634].

Giovannetti F., Kirchner M., Rockendorf G., Kehl O., 2011. Cellulose Triacetate Honeycomb Compounds for Improved Flat-Plate Collectors: Performance and Reliability. 30th ISES Biennial Solar World Congress 2011, SWC 2011.

Kalogirou S., 2003. The potential of solar industrial process heat applications. Applied Energy 76, 337-361.

Kessentini H., Capdevila R., Castro J., Oliva A., Bouden C., 2014. Three dimensional heat transfer analysis of combined conduction and radiation in honeycomb transparent insulation. Solar Energy 105, 58-70.

Kessentini H., Castro J., Capdevila R., Oliva A., 2014. Development of flat plate solar collector with plastic transparent insulation and low-cost overheating protection system. Applied Energy 133, 206-223.

Kizildag, D., Lehmkuhl, O., Rigola, J., Capdevila, R., Oliva, A., 2015. Thermal optimization of multi-functional façades as energy efficient solution in retroffiting public buildings, IPBSA, Hyderabad, India.

Lopez J., Lehmkuhl O., Damle R., Rigola J., 2012. A parallel and object-oriented general purpose code for simulation of multiphysics and multiscale systems. 24th Int. Conference on Parallel CFD, Atlanta.

Martínez A, Astrain D, Rodríguez A, Aranguren P., 2013. Thermoelectric self-cooling system to protect solar collectors from overheating. Journal of Electronic Materials 43(6), 1480-1486.Nkwetta D.N., Smyth M.,2012. The potential applications and advantages of powering solar air-conditioning systems using concentrator augmented solar collectors. Applied Energy 89(1), 380-286.

Platzer W.J., 1992. Total heat transport data for plastic honeycomb-type structures. Solar Energy 49(5), 351-358.

Rommel M., Wagner A.,1992. Application of transparent insulation materials in improved flat-plate collectors and integrated collector storages. Solar Energy 49(5), 371-380.

Sharma A.K., Sharma C., Mullick S.C., Kandpal T.C., 2017. Solar industrial process heating: A review. Renewable and Sustainable Energy Reviews 78, 124-137.

TIGI LTD., 2011. System and method for temperature limiting in a sealed solar energy collector. WO/2011/086534, A1: 1-40.